Vibrational Analysis of the Hydrogen-Bond Symmetrization in Ice

Xue Z. Lu,[†] Ying Zhang,*[,†] Peng Zhao,[†] and Shao J. Fang[‡]

School of Science, University of Jinan, Jinan 250022, China, and School of Physics and Microelectronics, National Key Laboratory of Crystal Materials, Shandong University, Jinan 250100, China

Received: August 7, 2010; Revised Manuscript Received: December 5, 2010

This paper presents a calculation of the vibrational spectra of hydrogen atoms and the probability distributions for protons along the hydrogen bonds to study the hydrogen-bond symmetrization in ice by performing ab initio molecular dynamics simulations. The disappearance of the translational peaks of ice VIII is observed, which is interpreted as a transition into disordered ice VII. Two peaks of the translational modes related to the hydrogen bond are observed again in the megabar range; meanwhile, a new band becomes a definite peak, which is assigned to the IR-active translational vibrational mode of ice X, both strongly indicating that a phase transition to ice X has occurred. Moreover, the proton probability distributions that can locate the proton position provide an intuitive way to understand the symmetrization process. The results give the reasonable interpretations of the conclusions obtained from the vibrational spectra of hydrogen atoms.

Introduction

Ice shows a complex behavior in the pressure−temperature phase diagram. Because the properties of the high-pressure ice can shed light onto the evolution of chemical bonding as well as the quantum effects of hydrogen, such as tunneling, we are confronted with a large number of theoretical and experimental studies. As early as 1972, Holzapfel[1] predicted that a high-pressure phase of H_2O should exist in which hydrogen-bonded protons would reside in the symmetric midpoints, leading the crystallographic nature of ice to change from the molecular phase to the atomic phase. This atomic phase was called ice X, or symmetric ice. Later, considerable discussions in the literature have detected the VII/VIII → X transition. There was a debate on the hydrogen-bond symmetrization process. So far, three different theories exist: (1) ice VII/VIII is directly transformed into ice X,[2−9] (2) ice VII/VIII is transformed into ice X via an intermediate phase characterized by dynamical disorder arising from the proton tunneling at low temperature and the thermal hopping of the proton at room temperature,[10−18] and (3) in recent years, the transformation to ice X through the sequence of ice VII/VIII → disordered ice VII → disordered ice X → ice X was suggested.[19−22] The characteristic feature of disordered ice VII is the same as that mentioned in (2). Disordered ice X is characterized as a unimodal distribution of the proton centered between two neighboring oxygen atoms, but the underlying potential is still of double-well type. However, the transition to ice X is still not fully understood. One of the reasons is a lack of experimental knowledge of the positions of the protons in the high-pressure phase. X-ray diffraction measurement is unable to probe the proton positions directly, even though it can suggest changes of the proton positions.[23] The neutron diffraction measurements that are capable of locating the H positions are limited to the study of the pressure to no more than 20 GPa.[24−26]

In this paper, we present the vibrational spectra of hydrogen atoms and the probability distributions for protons along the hydrogen bonds obtained by using the ab initio software package VASP based on density functional theory to study the dynamical properties of high-pressure ice. The vibrational spectra of hydrogen atoms give more vibrational signals of ice than IR and Raman simulations in the megabar range. In the vibrational spectra, the translational modes related to the hydrogen bond are observed in the megabar range, which are the new signatures of the transformation into ice X. The proton probability distributions allow us to analyze the location of the proton, giving us an intuitive way to understand the symmetrization process. Results show that the transformation to ice X follows the sequence, ice VIII → disordered ice VII → ice X.

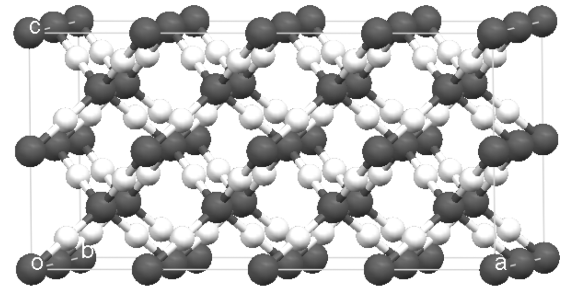

Figure 1. Structure of ice X. The unit cell has 32 H_2O molecules.

Computational Methods

Ice VIII consists of two interpenetrating ice I_c structures, where the hydrogen atoms are ordered and the body-centered cubic (bcc) sublattice of oxygen atoms has a small tetragonal distortion.[5,27] As in ref 5, the ice VIII structure without the small tetragonal distortion can be converted into the ice X structure by displacing the hydrogen atoms from the midpoints between two neighboring oxygen atoms. The ab initio molecular dynamics simulations (MD) were carried out on the supercell of 32 molecules initially arranged in the ice X,[5] as depicted in Figure 1. The density functional calculations were performed with the VASP codes[28] based on the plane-wave basis set, ultrasoft pseudopotentials,[29] and the PW91 functional.[30] The wave functions were expanded in plane waves at the Γ point using a cutoff of 400 eV. We performed the simulations at lattice

* To whom correspondence should be addressed. E-mail: ss_zhangy1@ujn.edu.cn (Y.Z.).
† University of Jinan.
‡ Shandong University.

10.1021/jp1074434
Published on Web 12/13/2010

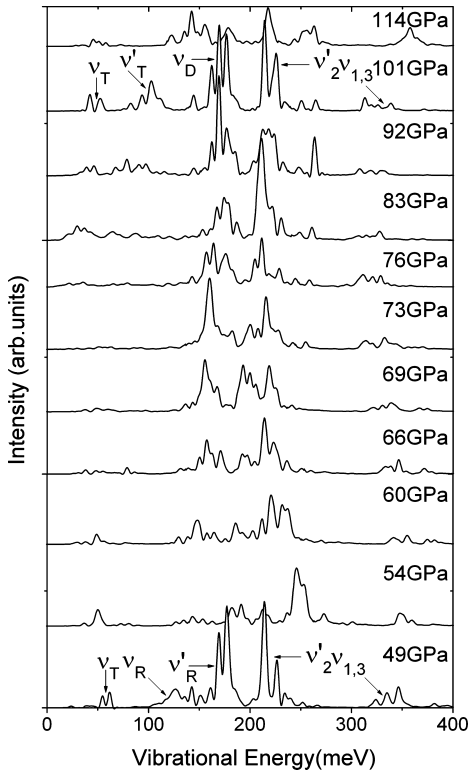

Figure 2. Vibrational spectra of hydrogen atoms.

constants from 2.62 to 2.82 Å in steps of 0.02 Å. The corresponding pressures were obtained using the experimental equation of state.[31] The temperature was set at 50 K in the microcanonical ensemble. The system was equilibrated for 1 ps, and data collection runs were performed for 6 ps, with a time step of 1 fs. In our simulations, the hydrogen atoms were treated as classical particles. The vibrational spectra of hydrogen atoms were obtained by performing Fourier transformation of velocity autocorrelation functions. Comparisons between the results obtained by ab initio MD simulations and the experiments described in refs 13 and 16 showed that the simulations with classical protons could well reproduce the main features of the experimental data. Comparisons between the quantum simulations and the classical simulations[19] also showed that the simulations at the classical level reproduce the qualitative features of the symmetrization process, and the quantum effects mainly influence the transition pressures shifting to lower pressures. Therefore, the transition pressures may be higher due to the neglect of the quantum effects in our study.

Results and Discussion

Vibrational Spectra of Hydrogen Atoms. The vibrational spectra of hydrogen atoms shown in Figure 2 are calculated over the range of 49−114 GPa. Compared with the Raman spectra,[14] we find that the vibrational spectrum of hydrogen atoms at 49 GPa resembles the corresponding spectrum of ice VIII in Raman data. On the other hand, we optimized the initial configuration (ice X) at 49 GPa. The optimized structure with the hydrogen atoms located at the positions about 42% of the O−O distances was characterized by the two interpenetrating, but unconnected, sublattices of the oxygen atoms, which was consistent with the structure of ice VIII. At 49 GPa, the high-energy O−H stretching vibrations in the vibrational spectrum form a triplet. Compared with the Raman data,[4,14] we can assign the observed triplet to $\nu_1(A_{1g})$, $\nu_3(E_g)$, and $\nu_1(B_{1g})$ modes in the order of increasing energy. We observe three vibrational bands at intermediate energies. The 220 meV band is the bending mode ν'_2 corresponding to ν_2, $\nu_2 + \nu_{T'}$, and $\nu_2 + \nu_{T''}$ in Raman data;[14] the lower-energy modes are the rotational vibrations, which are ν'_R ($\nu_{2R'}$ and $\nu_{2R''}$ in Raman data[14]) and ν_R. In the low-energy region, we observe two peaks at 55 and 62 meV, which are identified as the translational modes ν_T related to the hydrogen bond.

As shown in Figure 2, anomalies in the behavior of the translational modes of ice VIII, which are related to the hydrogen bond, are observed in the vibrational spectra. At 49 GPa, two well-resolved translational peaks are observed. With increasing pressure, these two peaks shift to low energy up to 54 GPa. In the range of 54−69 GPa, the translational peaks exhibit minor energy shifts. As for the intensity of the two translational peaks, the lower-energy translational peak shows a rapid decrease up to 54 GPa and then a very slight change in intensity with increasing pressure, whereas the intensity of the upper energy translational peak gradually decreases above 54 GPa, and then both translational peaks disappear at about 73 GPa. The similar changes in the translational peaks have been observed in Raman measurements.[12,14] The disappearance of the translational peaks at about 73 GPa, which results from the strong proton disorder, as discussed in the following section, is interpreted as a transition from ice VIII to disordered ice VII. With the increasing pressure, two peaks located at about 41 and 51 meV are observed again in the spectrum at 101 GPa. This spectral feature can be interpreted as a transition into a new phase, ice X. The translational modes of ice X have not been detected in the megabar range in Raman measurements.[4,12,14] As for IR measurements,[6−9,15,17,20] they are limited to the study of the low-energy region (<88 meV). In the ab initio study of IR spectra,[13] the experimental gap was filled. A translational mode was observed in the low-pressure range, but it disappeared in the megabar range.

In addition, a new peak appears in the low-energy region around 83 GPa and exhibits its whole peak shape around 100 meV at 101 GPa. The IR measurements[8,20] demonstrate that only two peaks are IR-active in ice X. One named ν'_T translational mode is a translational vibration associated with opposite displacements of hydrogen and oxygen atoms, and the other one named ν_D distortional mode is a distortional twisting of the tetrahedron of hydrogen atoms around a resting oxygen atom. They are located at about 113 and 175 meV in the IR spectrum, respectively.[8,20] The peak located at 100 meV in our spectrum at 101 GPa corresponds to the ν'_T translational mode, which appears in the low-energy region and becomes a definite peak in the megabar range in the IR spectra.[8,20] We, therefore, confirm that the new peak at 100 meV is another spectral feature indicating occurrence of the hydrogen-bond symmetrization. The ν_D distortional mode located at 173 meV is also observed in our spectrum at 101 GPa. This mode was predicted to originate from the rotational modes (ν'_R and ν_R) of ice VIII.[17,20] On comparison of the spectrum at 49 GPa with that at 101 GPa, it seems that the rotational modes (ν'_R and ν_R) of ice VIII are converted into the ν_D distortional mode in our spectra.

In our calculated spectra, the ν'_2 bending mode shows a pressure-insensitive behavior that is consistent with the experimental data.[8,17] The difference between the calculated and the experimental data is that the ν'_2 bending mode exists over the whole pressure range in our spectra. In contrast to the pressure-insensitive behavior of the ν'_2 bending mode, the O−H stretching modes exhibit a softening behavior up to 83 GPa,

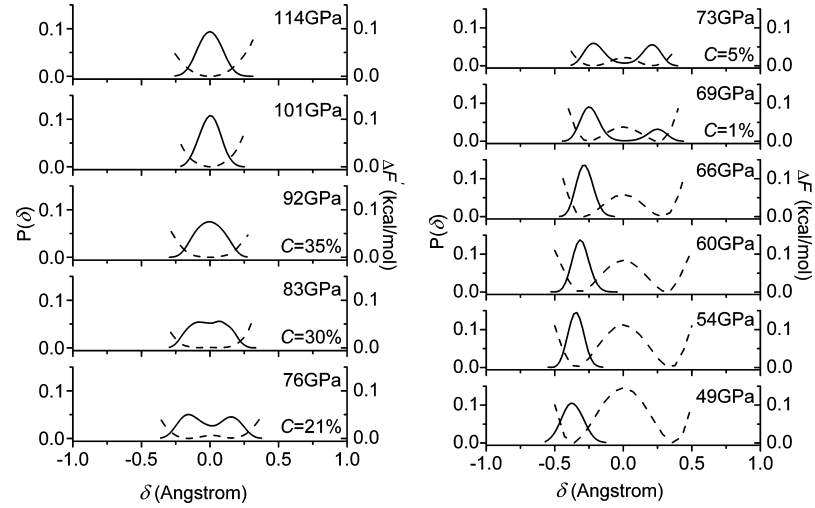

Figure 3. Probability distributions for protons along the hydrogen bonds $P(\delta)$ (solid lines and left axis) and scaled free energy profiles for protons along the hydrogen bonds $\Delta F'(\delta) = \Delta F(\delta)/10$ (dashed lines and right axis), where $\delta = R_{O_aH} - R_{O_bH}$ and $\delta = 0$ indicates the midpoint of the hydrogen-bonded O_a-O_b distance. $\Delta F(\delta)$ is scaled in order to display it on the same scale as $P(\delta)$. The relative number of ionic defects, C, from 69 to 92 GPa, which is defined as $\langle n_{broken}\rangle/n_{sites}$, is obtained by the number of broken water molecules (based on a geometric criterion) divided by the number of available lattice sites.[16]

but the magnitudes of decrease are much less than that observed in the experiments.[8,17] In addition, the O−H stretching modes shift to high energy with increasing pressure above 83 GPa, which differs from the disappearance of the O−H stretching modes in the experimental data.[8,17]

So far, no inelastic neutron scattering data, which can give more detailed vibrational signals, have yet been reported for ice X. Detailed comparisons between our spectra and the IR experimental spectra[8,17] are discussed above. More vibrational signals are observed in the megabar range in our spectra. There are five vibrational modes in our spectra of ice X, as indicated in Figure 2, whereas in the IR spectra,[8,20] only two peaks were observed in ice X, which were ν'_T translational and ν_D distortional modes in the order of increasing energy. When the neutron scattering measurement is available at high pressure (>100 GPa) in the future, we may compare our vibrational spectra with the neutron scattering spectra in detail.

Probability Distributions for Protons along the Hydrogen Bonds. The three stages, "ice VIII → disordered ice VII → ice X", are clearly observed in the probability distributions for protons along the hydrogen bonds. The probability distributions for protons (solid lines) and the free energy profiles for protons (dashed lines), that is, proton-transfer potential, are shown in Figure 3. Below 69 GPa, the potential is of the double-well type, and the barrier decreases with increasing pressure. Meanwhile, the proton probability distributions are found to be unimodal with one peak close to a given oxygen atom, indicating that the hydrogen atoms remain attached to a given oxygen atom and this system is ice VIII. At 69 GPa, the proton probability distribution becomes a bimodal distribution; the hydrogen atoms start to jump as indicated in Figure 4. With increasing pressure, the potential barrier continues to decrease and the hydrogen atoms exchange their positions constantly by traveling back and forth along their hydrogen bonds, which results in strong proton disorder, as shown in Figure 4. Above 69 GPa, the proton probability distribution gradually changes from double peak to single peak with an increase in pressure. At 92 GPa, the potential barrier disappears, which indicates the formation of the single-well potential, but the bottom of the potential is so flattened that the hydrogen atoms are still delocalized in a large extent along the hydrogen bonds. Therefore, although a unimodal proton distribution is observed at 92 GPa, the width of the peak is still wide and the top of the peak is still flat. On further compression, when the pressure is 101 GPa, the single-well potential narrows and the hydrogen atoms are localized at the

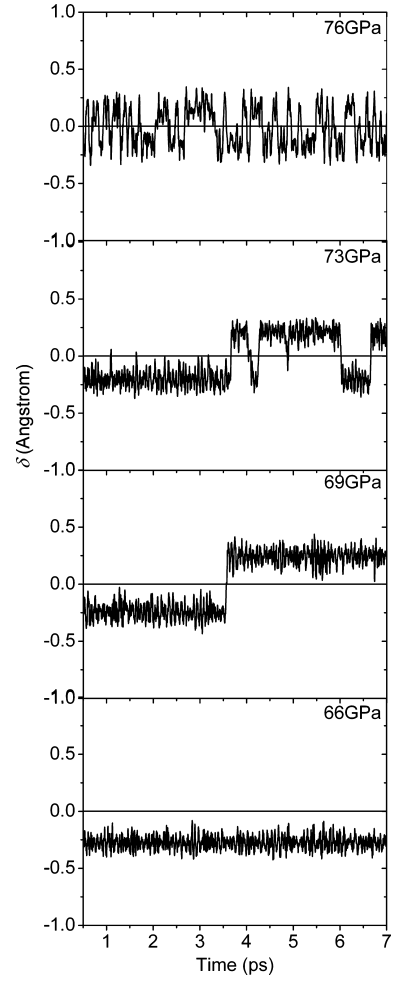

Figure 4. Coordinates for proton transfer $\delta = R_{O_aH} - R_{O_bH}$ are plotted as a function of the simulation time. The horizontal bars indicate the midpoints of the hydrogen-bonded O_a-O_b distances at the corresponding pressures.

midpoints of the hydrogen bonds. A narrow unimodal proton distribution is observed. The emerging structure is isostructural to the static cuprite structure, indicating the formation of ice X. It is to be noted that the pressure of the ice VIII → disordered ice VII transformation at 69 GPa determined by the proton probability distributions is lower than 73 GPa obtained using our calculated spectra. This phenomenon can be reasonably understood. Although the hydrogen atoms start to hop between two symmetric sites along the hydrogen bonds at 69 GPa, only a single proton hop occurs during the simulation time of 6 ps, as indicated in Figure 4. This phenomenon shows a very weak proton disorder at the onset of the disordered ice VII. Therefore, it probably leads to an insensitive behavior at 69 GPa and thus a higher transition pressure in the calculated spectra.

In disordered ice VII, it consists of H_2O, H_3O^+, and OH^- ionic defects.[10,16,18] As an important property of disordered ice VII, the H_3O^+ and OH^- ionic defects are also investigated in our system. We calculate the ionic defects following along the lines of the analysis presented in ref 16. The results shown in Figure 3 from 69 to 101 GPa indicate an increasing tendency of the relative number of ionic defects *C*, which is consistent with the conclusion obtained from ref 16. This implies that the ice rules are violated in this phase, but the hydrogen atoms still have a significant amount of short-range order so as to form intact water molecules.[10]

A disordered symmetric phase (disordered ice X) has been predicted to appear prior to the transition to ice X.[19] On the basis of the analysis of the vibrational spectra of hydrogen atoms and proton probability distributions, we have not observed a remarkable change corresponding to the transition to the disordered ice X in our spectra, such as the disappearance of one vibrational mode, as discussed in ref 20. The IR measurement[17] and ab initio calculation of the IR spectrum[13] have been reported to study the hydrogen-bond symmetrization process. There was also no evidence of the transition to the disordered ice X in their IR spectra.

Conclusions

The ab initio simulations reported here reveal that the hydrogen-bond symmetrization process is the following: ice VIII → disordered ice VII → ice X. The signatures in the vibrational spectra of the transformation into ice X are identified. The disappearance of the translational peaks of ice VIII is considered as a signature of the transition into disordered ice VII; hereafter, the appearance of the translational peaks of ice X, which are related the hydrogen bond, strongly indicates the transition into ice X. In agreement with the experimental data,[20] a new peak at 100 meV is another signature of the transition to ice X. Meanwhile, analysis of the proton probability distributions gives an intuitive way to understand the symmetrization process. The results add further support to the signatures of the ice VIII → disordered ice VII and disordered ice VII → ice X transformations in the spectra.

Acknowledgment. The authors thank the School of Physics and Microelectronics, National Key Laboratory of Crystal Materials, Shandong University, China, for the use of their supercomputers. The work was supported, in part, by the Natural Science Foundation of Shandong Province of China (Grant No. ZR2009AL004) and the Doctoral Foundation of the University of Jinan, China (Grant No. B0623).

References and Notes

(1) Holzapfel, W. B. *J. Chem. Phys.* **1972**, *56*, 712.
(2) Walrafen, G. E.; Abebe, M.; Mauer, F. A.; Block, S.; Piermarini, G. J.; Munro, R. *J. Chem. Phys.* **1982**, *77*, 2166.
(3) Polian, A.; Grimsditch, M. *Phys. Rev. Lett.* **1984**, *52*, 1312.
(4) Hirsch, K. R.; Holzapfel, W. B. *J. Chem. Phys.* **1986**, *84*, 2771.
(5) (a) Lee, C.; Vanderbilt, D.; Laasonen, K.; Car, R.; Parrinello, M. *Phys. Rev. Lett.* **1992**, *69*, 462; *Phys. Rev. B* **1993**, *47*, 4863.
(6) Aoki, K.; Yamawaki, H.; Sakashita, M. *Phys. Rev. Lett.* **1996**, *76*, 784.
(7) Goncharov, A. F.; Struzhkin, V. V.; Somayazulu, M. S.; Hemley, R. J.; Mao, H. K. *Science* **1996**, *273*, 218.
(8) Aoki, K.; Yamawaki, H.; Sakashita, M.; Fujihisa, H. *Phys. Rev. B* **1996**, *54*, 15673.
(9) Struzhkin, V. V.; Goncharov, A. F.; Hemley, R. J.; Mao, H. K. *Phys. Rev. Lett.* **1997**, *78*, 4446.
(10) Schweizer, K. S.; Stillinger, F. H. *J. Chem. Phys.* **1984**, *80*, 1230.
(11) Wolanin, E.; Pruzan, Ph.; Chervin, J. C.; Canny, B.; Gauthier, M.; Hausermann, D.; Hanfland, M. *Phys. Rev. B* **1997**, *56*, 5781.
(12) Pruzan, Ph.; Wolanin, E.; Gauthier, M.; Chervin, J. C.; Canny, B.; Hausermann, D.; Hanfland, M. *J. Phys. Chem. B* **1997**, *101*, 6230.
(13) Bernasconi, M.; Silvestrelli, P. L.; Parrinello, M. *Phys. Rev. Lett.* **1998**, *81*, 1235.
(14) Goncharov, A. F.; Struzhkin, V. V.; Mao, H. K.; Hemley, R. J. *Phys. Rev. Lett.* **1999**, *83*, 1998.
(15) Katoh, E.; Song, M.; Yamawaki, H.; Fujihisa, H.; Sakashita, M.; Aoki, K. *Phys. Rev. B* **2000**, *62*, 2976.
(16) Benoit, M.; Romero, A. H.; Marx, D. *Phys. Rev. Lett.* **2002**, *89*, 145501.
(17) Song, M.; Yamawaki, H.; Fujihisa, H.; Sakashita, M.; Aoki, K. *Phys. Rev. B* **2003**, *68*, 014106.
(18) Goncharov, A. F.; Goldman, N.; Fried, L. E.; Crowhurst, J. C.; Kuo, I.; Feng, W.; Mundy, C. J.; Zaug, J. M. *Phys. Rev. Lett.* **2005**, *94*, 125508.
(19) Benoit, M.; Marx, D.; Parrinello, M. *Nature* **1998**, *392*, 258.
(20) Song, M.; Yamawaki, H.; Fujihisa, H.; Sakashita, M.; Aoki, K. *Phys. Rev. B* **1999**, *60*, 12644.
(21) Benoit, M.; Marx, D. *ChemPhysChem* **2005**, *6*, 1738.
(22) Sugimura, E.; Iitaka, T.; Hirose, K.; Kawamura, K.; Sata, N.; Ohishi, Y. *Phys. Rev. B* **2008**, *77*, 214103.
(23) Loubeyre, P.; LeToullec, R.; Wolanin, E.; Hanfland, M.; Hausermann, D. *Nature* **1999**, *397*, 503.
(24) Nelmes, R. J.; Loveday, J. S.; Wilson, R. M.; Besson, J. M.; Pruzan, Ph.; Klotz, S.; Hamel, G.; Hull, S. *Phys. Rev. Lett.* **1993**, *71*, 1192.
(25) Besson, J. M.; Pruzan, Ph.; Klotz, S.; Hamel, G.; Silvi, B.; Nelmes, R. J.; Loveday, J. S.; Wilson, R. M.; Hull, S. *Phys. Rev. B* **1994**, *49*, 12540.
(26) Nelmes, R. J.; Loveday, J. S.; Marshall, W. G.; Hamel, G.; Besson, J. M.; Klotz, S. *Phys. Rev. Lett.* **1998**, *81*, 2719.
(27) Kuhs, W. F.; Finney, J. L.; Vettier, C.; Bliss, D. V. *J. Chem. Phys.* **1984**, *81*, 3612.
(28) Kresse, G.; Hafner, J. *Phys. Rev. B* **1994**, *49*, 14251. Kresse, G.; Furthmüller, J. *Comput. Mater. Sci.* **1996**, *6*, 15. Kresse, G.; Furthmüller, J. *Phys. Rev. B* **1996**, *54*, 11169.
(29) Vanderbilt, D. *Phys. Rev. B* **1990**, *41*, 7892.
(30) Perdew, J. P.; Wang, Y. *Phys. Rev. B* **1992**, *45*, 13244. Perdew, J. P.; Chevary, J. A.; Vosko, S. H.; Jackson, K. A.; Pederson, M. R.; Singhm, D. J.; Foihairs, C. *Phys. Rev. B* **1992**, *46*, 6671.
(31) Hemley, R. J.; Jephcoat, A. P.; Mao, H. K.; Zha, C. S.; Finger, L. W.; Cox, D. E. *Nature* **1987**, *330*, 737.

JP1074434